

Gas and Metal Contents of Galaxies and Gaseous Halos: Preventive versus Ejective Feedback

Yu Lu^{1*}, H.J. Mo², Zhankui Lu²

¹ *Observatories, Carnegie Institution for Science, 813 Santa Barbara Street, Pasadena, CA 91101, USA*

² *Department of Astronomy, University of Massachusetts, Amherst MA 01003-9305, USA*

ABSTRACT

Using a semi-analytical approach we investigate the characteristics of predictions for the masses and metallicities of the baryonic matter in and around galaxies made by three galaxy formation models. These models represent three different feedback scenarios: one model with purely ejective feedback, one model with ejective feedback with reincorporation of ejected gas, and one preventative model. We find that, when the model parameters are adjusted to predict the correct stellar masses for a range of halo masses between 10^{10} to $10^{12} M_{\odot}$, these three scenarios have very different predictions for the masses and metallicities of the interstellar and circum-galactic media. Compared with current observational data, the model implementing preventative feedback has a large freedom to match a broad range of observational data, while the ejective models have difficulties to match a number of observational constraints simultaneously, independent of how the ejection and reincorporation are implemented. Our results suggest that the feedback process which regulates the amounts of stars and cold gas in low-mass galaxies is preventative in nature.

Key words: galaxies: evolution; galaxies: formation; galaxies:ISM; galaxies: stellar content

1 INTRODUCTION

One of the most fundamental questions in galaxy formation is how baryons are accreted into and expelled from dark matter halos as galaxies form. Using statistical approaches, a number of studies have revealed a picture in which the baryonic mass locked into stars and cold gas is a strong function of galaxy mass (Yang, Mo & van den Bosch 2003; Behroozi, Conroy & Wechsler 2010; Moster, Naab & White 2013; Papastergis et al. 2012; Lu et al. 2014b). The Milky Way sized galaxies at the present day have the largest baryon mass fraction in stars, and this fraction decreases rapidly as the galaxy mass increases and decreases. How such a relation is established is one of the most important questions in galaxy formation. A widely adopted galaxy formation scenario attributes the low baryon mass fraction in low-mass halos to strong galactic outflows generated by the feedback of star formation (e.g. Dekel & Silk 1986; Bower et al. 2006; Croton et al. 2006). On the other hand, a number of authors have realized that preventing baryons from ever collapsing into dark matter halos may also be a viable solution (Mo & Mao 2002; Benson & Madau 2003; Mo & Mao 2004; van den Bosch, Abel & Hernquist 2003; Oh & Benson 2003; Mo et al. 2005; Lu & Mo 2007; Lu, Mo & Wechsler

2015). Clearly, how feedback works in reality becomes a central question in galaxy formation theory. In this paper, we present a comparative study of three representative feedback models to understand the impact of ejective versus preventative feedback scenarios on their predictions for the masses and metallicities in different components of disk galaxies.

The details of feedback processes are still poorly understood. In the commonly adopted ejective scenario, feedback of star formation is assumed to produce strong outflows which can expel a large amount of gas mass from the host halo (e.g. Benson et al. 2003; Somerville et al. 2008; Guo et al. 2011). However, the properties of the outflows, such as their masses and velocities, and how they are coupled to the halo gas are still uncertain. More recently, a more sophisticated scenario, in which ejected gas is allowed to reincorporate back to the host halo after a certain time scale is proposed (e.g. Henriques et al. 2013). In addition to the same uncertainties that the simple ejective model has, the ejective model with reincorporation also has uncertainties in the time scale for the gas reincorporation. The physics of these assumed processes is still poorly understood. In the preventative scenario, some early feedback is assumed to change the thermal state of the intergalactic medium around dark matter halos so that a fraction of baryons is prevented from collapsing into dark matter halos in the first place. For example, as shown in Lu, Mo & Wechsler (2015), when the

* E-mail: luyu@carnegiescience.edu

circum-halo medium is preheated by early feedback to a certain level of entropy, the thermal pressure of the preheated gas can support the gas against gravitational pull, resulting in a low baryon mass fraction for low-mass halos. As demonstrated in Lu, Mo & Wechsler (2015), such a model seems to be able to reproduce the observed stellar and cold gas mass fractions, sizes of disk galaxies, and star formation histories of galaxies with mass comparable to or lower than the Milky Way, without invoking any strong outflow as adopted in the ejective scenario. An important question is then whether these different feedback scenarios can be distinguished with current observational data.

Metallicities in different phases of a galaxy is expected to put interesting constraints on feedback models. Metals are produced by star formation and their distribution is affected by feedback. If, for example, the feedback drives weak outflows, metals would be found only in regions where star formation has taken place. On the other hand, if strong outflows are driven to large distances, metals produced by star formation can be redistributed not only in ISM (cold gas) but also in the hot halo gas and even in the intergalactic medium. In this paper, we adopt a semi-analytic galaxy formation model introduced in Lu, Mo & Wechsler (2015) to better understand how the masses and metallicities of baryonic matter in different phases are affected by different implementations of feedback. The goal is to examine how current and future observations may be used to distinguish between different feedback scenarios.

The paper is organized as follows. In §2, we describe the models adopted in this paper. We present our model predictions and comparisons with observations for the evolution of the baryonic masses in different components in §3, and for the metallicities in different phases in §4. Our conclusions and the discussion of the implications of the results are presented in §5. Throughout the paper, we use a Λ CDM cosmology with $\Omega_{M,0} = 0.27$, $\Omega_{\Lambda,0} = 0.73$, $\Omega_{B,0} = 0.044$, $h = 0.70$, $n = 0.95$, and $\sigma_8 = 0.82$.

2 MODELS

We adopt the semi-analytical model (SAM) introduced in Lu, Mo & Wechsler (2015) and focus on different implementations of star formation feedback. To do this, we fix every other parts of the model, but vary the recipe for star formation feedback to study the impact of feedback on the observational consequences of the masses and metallicities in stars, ISM and circum-galactic medium (CGM). We concentrate on galaxies with mass comparable to or smaller than that of the Milky Way. We consider three representative models, which differ from each other by their assumptions on how feedback governs gas inflow and outflow.

The first model is a typical ejective feedback model presented in Lu, Mo & Wechsler (2015). This model, referred to as Model-EJ in the following, captures the essence of many ejective feedback models in the literature in terms of how outflows driven by star formation feedback affect the baryon contents of low-mass galaxies (e.g. Bower et al. 2006; Kang, Jing & Silk 2006; Somerville et al. 2008). Halos are assumed to accrete baryons at a rate equal to the halo mass accretion rate multiplied by the universal baryon fraction $f_b = \Omega_{B,0}/\Omega_{M,0}$, and a certain fraction of cold gas

is assumed to be ejected out of the host halo as stars form. The ejected mass is assumed to be proportional to the star formation rate with a mass-loading factor that varies with the halo virial velocity V_{vir} . Based on the energy conservation argument, the mass-loading factor is assumed to be inversely proportional to V_{vir}^2 and the mass ejection rate is written as

$$\dot{M}_{\text{ej}} = \psi \alpha_{\text{LD}} \left(\frac{200 \text{km/s}}{V_{\text{vir}}} \right)^2, \quad (1)$$

where ψ is the star formation rate (SFR), and α_{LD} is the normalization of the mass-loading factor at $V_{\text{vir}} = 200 \text{ km/s}$. The ejected mass is assumed to leave the halo and is added into an ‘ejected mass’ component. For the model considered here, we assume that the ejected mass never comes back to the halo to explore the maximum effect of the ejective feedback scenario. Based on these assumptions, the mass of the hot halo gas is given by

$$M_{\text{hot}} = f_b M_{\text{vir}} - M_* - M_{\text{cold}} - M_{\text{ej}}, \quad (2)$$

where M_{vir} is the virial mass of the halo, M_* is the stellar mass and M_{cold} is the cold gas mass of the galaxy. The normalization factor, α_{LD} , is tuned so that the model prediction matches the stellar mass of Milky Way sized halos as derived from recent empirical models that match galaxy stellar mass functions at multiple redshifts (Behroozi, Wechsler & Conroy 2013; Lu et al. 2014a). We find that $\alpha_{\text{LD}} = 1$ provides a reasonable fit to both the stellar mass and cold gas mass in Milky Way sized halos. Since the mass loading factor scales as V_{vir}^{-2} , lower-mass halos have larger mass-loading factors. Moreover, in order to explain the metal mass in the circum-galactic medium (CGM), we deposit a fraction, α_Z , of the metal yield from star formation directly into the hot halo gas, and the rest is mixed uniformly into the ISM before being ejected out of the halo. We explore the effect of changing the fraction of this direct metal injection into the halo gas and found that $\alpha_Z = 0.1$ produces a good match to the OVI gas mass observed in COS-Halos, assuming the OVI ionization fraction $f_{\text{OIV}} = 0.2$ (Tumlinson et al. 2011). A lower level of direct metal injection would predict a too low oxygen mass to be consistent with the observational constraints.

The second model considered here is an extended ejective model, in which the ejected gas mass is allowed to reincorporate into the halo hot gas after a period of time. Specifically, we implement the model proposed by Henriques et al. (2013), where the gas reincorporation rate is written as

$$\dot{M}_{\text{ej}} = -\frac{M_{\text{ej}}}{t_{\text{reinc}}}, \quad (3)$$

where t_{reinc} is the time scale for the ejected gas to fall back into the halo. Henriques et al. (2013) utilized a MCMC method to optimize a flexible version of the L-Galaxies SAM to match the evolution of galaxy luminosity function, and found the following model for t_{reinc} :

$$t_{\text{reinc}} = \gamma \frac{10^{10} M_{\odot}}{M_{\text{vir}}}, \quad (4)$$

where γ is a free parameter tuned to be $\gamma = 1.8 \times 10^{10} \text{ yr}$. To be consistent with the Henriques model, the prescription and parameter values of the outflow model we adopt follow Henriques et al. (2013) exactly. Specifically, a fraction

of cold gas is assumed to be heated and deposited into the hot halo gas reservoir and another fraction is assumed to be ejected and leave the halo. The ejected gas is then subject to reincorporation. The details of the model parameterization can be found in Guo et al. (2011), and the detailed modeling of the reheating, ejection and reincorporation can be found in Henriques et al. (2013). In what follows, this model is referred to as Model-RI. Because this model already has reheated ISM to be mixed with the halo gas, we do not assume any additional channel of metal injection into the hot halo.

The third model is the preventative feedback model introduced in Lu, Mo & Wechsler (2015). In this model, the effect of feedback is not to eject gas out of halos but to prevent a fraction of the baryonic matter from collapsing into halos. This is achieved by assuming that the intergalactic medium (IGM) is pre-heated to a certain entropy level so that a fraction of baryonic mass will not be able to collapse into the shallow gravitational potential wells of low-mass halos owing to the thermal pressure of the preheated gas. As demonstrated with hydrodynamical simulations in Lu & Mo (2007), a uniform entropy distribution of the IGM results in the fraction of baryon mass that collapses into a halo to be proportional to the halo mass squared, $M_b \propto M_{\text{vir}}^2$, which is needed to match the shallow low-mass end slopes of local galaxy stellar mass and HI-mass functions (Mo et al. 2005). In addition, the halo gas in this model is assumed to establish a hot corona with an extended central core in its density profile. Lu, Mo & Wechsler (2015) showed that this preventative scenario can reproduce the observed cold gas mass, stellar mass, star formation history, and size for galaxies with masses comparable to or smaller than that of the Milky Way without invoking any outflow after preheating. On the other hand, however, such a universal prevention cannot suppress star formation sufficiently for more massive galaxies at late time. Thus, a “late quenching” process is needed for these galaxies. Here we consider a mechanism in which the stars and/or the central black hole in the central galaxy produce certain amounts of heating to offset the cooling of the halo gas. Motivated by the results of Lu & Mo (2014) that the classical bulge mass and central black-hole mass in a galaxy with total stellar mass $10^{10} M_\odot < M_* < 10^{11} M_\odot$ both scale roughly as M_*^2 , we assume that the heating rate depends on M_* as

$$\dot{H} = \epsilon \left(\frac{M_*}{10^{10} M_\odot} \right)^2 M_\odot \text{yr}^{-1}, \quad (5)$$

where the heating efficiency is set to be $\epsilon = 5$. In every time step, we calculate the halo cooling rate, \dot{C} , as described in Lu, Mo & Wechsler (2015), and the heating rate. The net cooling rate is then

$$\dot{M}_{\text{cool}} = \max[\dot{C} - \dot{H}, 0]. \quad (6)$$

Moreover, we also allow a moderate level of outflow, assuming a constant mass-loading factor of unity for all galaxies. This assumption is consistent with directly observations of outflows (e.g. Bouché et al. 2012; Kacprzak et al. 2014), and is also allowed by statistical inference from an empirical model of galaxy evolution constrained by stellar mass functions at different redshifts (Lu, Mo & Lu 2014). This model is referred to as Model-PR in the following.

For all the three models, we follow not only the mass

of baryonic matter in each phase as in Lu, Mo & Wechsler (2015), but also metallicities in the different phases. For all the phases considered here, namely the halo gas, cold gas, ejected gas, and stars, we only track the average metallicity for each phase, but do not follow the details of the metallicity distribution. Throughout the paper, we adopt the solar metallicity as $[12 + \log(\text{O}/\text{H})]_\odot = 8.69$ (Allende Prieto, Lambert & Asplund 2001; Asplund et al. 2009) and $Z_\odot = 0.0134$ (Asplund et al. 2009), and the total metal yield is taken to be $p = 0.03$, which is defined as the ratio between the mass of newly produced metals that are ejected into the ISM and the gas mass turned into stars. With the assumption that all galaxies have the same abundance ratio as the Sun, the oxygen yield is $p_{\text{oxy}} = 0.44p$.

3 BARYONIC MASSES IN DIFFERENT COMPONENTS

To understand how the baryonic masses in stars, cold gas, hot halo gas and ejected components evolve with time in different models, we apply these models to typical halo mass accretion histories (MAHs) of two final halo masses, $10^{11} M_\odot$ and $10^{12} M_\odot$. For simplicity, we adopt the fitting model of McBride, Fakhouri & Ma (2009),

$$M_{\text{halo}}(z) = M_{\text{halo},0} (1+z)^\alpha \exp(-\eta z), \quad (7)$$

where the normalization $M_{\text{halo},0}$ is the halo mass at $z = 0$ and the parameters α and η determine the shape of the MAH. This functional form can be considered as a generalization of two other widely adopted models proposed earlier by Wechsler et al. (2002) and van den Bosch (2002), and has been shown to accurately describe the assembly histories over a wide range of halo masses. It is also similar to other models proposed in the literature (Zhao et al. 2003a,b, 2009; Dekel et al. 2009). McBride, Fakhouri & Ma (2009) showed that the parameters α and η have broad distributions. For our model, we choose the typical values of these two parameters: $\alpha = 0.6$ and $\eta = 0.9$ for $M_{\text{halo},0} = 10^{12} M_\odot$ halos, and $\alpha = 0.8$ and $\eta = 0.9$ for $M_{\text{halo},0} = 10^{11} M_\odot$. This model matches well the simulated MAH, as shown in Lu, Mo & Wechsler (2015).

Following the spirit of SAM, we compute, at each time step, the halo gas accretion, hot gas distribution, radiative cooling, star formation and feedback, and keep track of the evolutions of the masses in stars, cold gas in the disk, hot gas in the halo, and the gas ejected out of the halo. The model predictions are shown in Figure 1, with the upper row for $M_{\text{halo},0} = 10^{11} M_\odot$ halos, and the lower row for $M_{\text{halo},0} = 10^{12} M_\odot$. While the three models predict similar albeit distinguishable histories for the stellar mass and cold gas mass, they predict very different histories for the halo gas and ejected gas masses. Model-EJ predicts the ejection of a large amount of gas and the ejected mass is kept out of the halo. Consequently the majority (more than half) of the baryonic mass originally associated with the halo is predicted to be ejected for both the halo masses. For $M_{\text{halo},0} = 10^{11} M_\odot$, the cold gas is the second dominating component, but for $M_{\text{halo},0} = 10^{12} M_\odot$, hot halo gas mass is comparable to the mass of the stellar component while the cold gas mass is the smallest of all. The

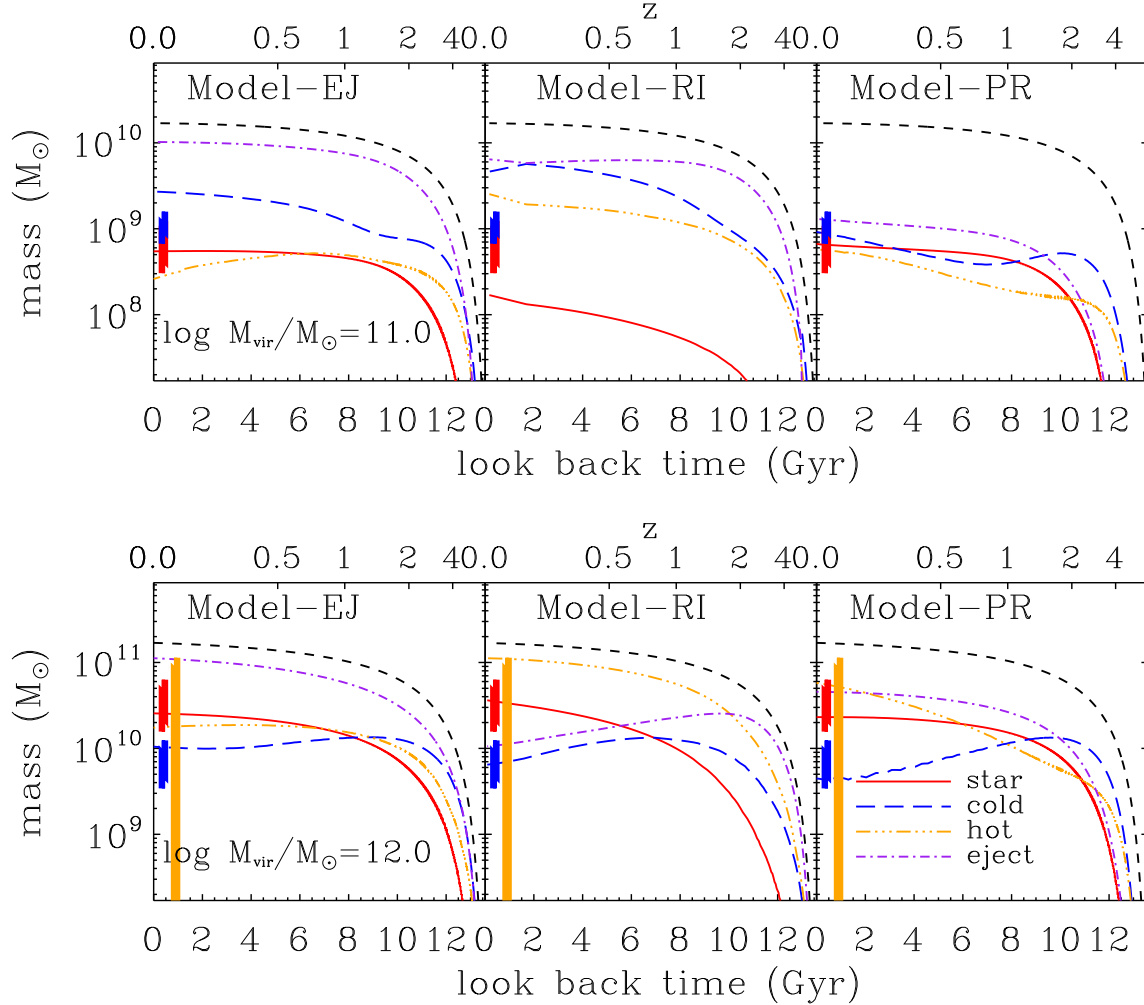


Figure 1. The mass of different baryonic component as a function of time (redshift) for halos with a final mass of $10^{12} M_{\odot}$ and $10^{11} M_{\odot}$ at the present day. The predictions of different models are labeled by their names in different panels. The red and blue lines show the stellar mass and the cold gas mass in model galaxies, respectively. The orange line is the gas mass in the hot halo, and the purple line is the mass ejected out of the halo. The black dashed line plots the halo mass multiplied by the cosmic baryon mass fraction f_b . The vertical bars mark the ranges of observational results. For stellar mass, the observational data constraint is taken from Behroozi, Wechsler & Conroy (2013) and Lu et al. (2014a). For the cold gas, the observational constraint is from Papastergis et al. (2012). The constraint for the hot halo gas is adopted by bracketing data constraints obtained from Fang et al. (2006) and Bregman & Lloyd Davies (2007).

ejected mass never decreases with time because of the absence of re-incorporation. The situation is very different in Model-RI. Although this model also implements a strong outflow, the ejected mass is re-incorporated back into the host halo at late times. Owing to the increasing reincorporation timescale with decreasing halo mass, the ejected gas outside the halo is always the dominating fraction for low-mass halos, but it is a significantly lower fraction for $M_{\text{halo},0} = 10^{12} M_{\odot}$. Furthermore, for the $10^{12} M_{\odot}$ halos in this model, the ejected mass dominates the baryon mass budget only at very early time ($z > 2$), and this fraction decreases rapidly at low redshifts as the halo mass increases to the regime where re-incorporation becomes important. Finally, for Model-PR, the total baryon mass budget is governed by the preheating entropy, which causes low-mass halos to be relatively poor in baryons. Since a low mass-loading factor of outflow is assumed in this model, the ejected mass

simply follows the stellar mass history with a delay caused stellar evolution (see Lu, Mo & Wechsler 2015, for details). For $M_{\text{halo},0} = 10^{11} M_{\odot}$, the cold gas mass is about $10^9 M_{\odot}$ at the present day, and the stellar mass is about half of the cold gas mass. For $M_{\text{halo},0} = 10^{12} M_{\odot}$, on the other hand, the stellar mass reaches about $3 \times 10^{10} M_{\odot}$ while the cold gas mass is about one order of magnitude lower. For both $M_{\text{halo},0} = 10^{11} M_{\odot}$ and $10^{12} M_{\odot}$, the hot halo gas mass is comparable to the stellar mass at the present time.

We compare the predicted stellar and cold gas masses at the present day with the results of Behroozi, Wechsler & Conroy (2013), Lu et al. (2014a) and Papastergis et al. (2012), shown as the vertical red and blue bars. The observational results for the hot halo gas are from Fang et al. (2006), Bregman & Lloyd Davies (2007), Yao et al. (2008), Tumlinson et al. (2011) and Gupta et al. (2012), and shown as the vertical yellow bars. Because

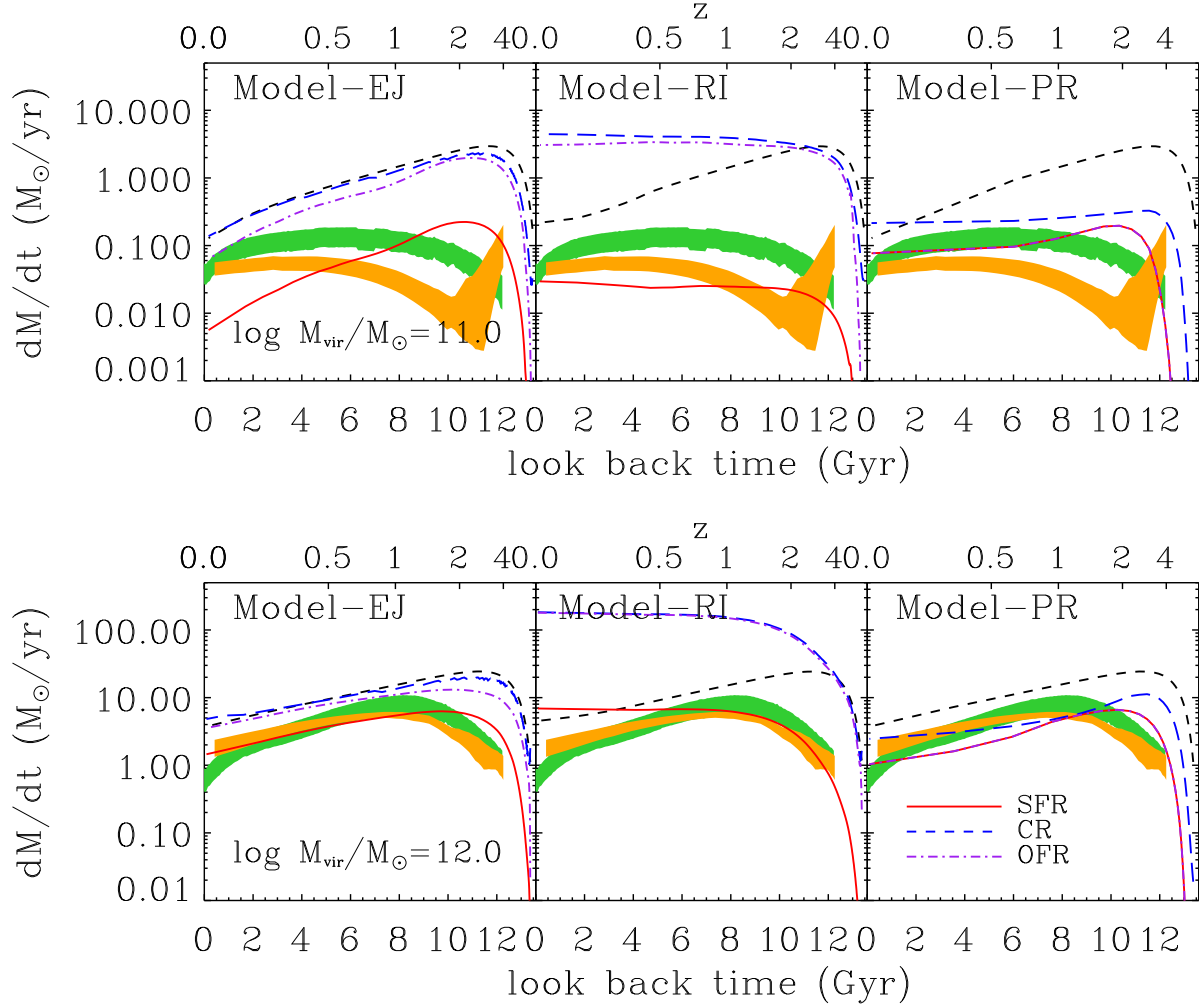


Figure 2. The rates of baryonic mass conversion among different phases as functions of time (redshift) for halos with a final mass of $10^{12} M_{\odot}$ and $10^{11} M_{\odot}$ at the present day. The predictions of different models are labeled by their names in different panels. The red line is the star formation rate; the blue line is the radiative cooling rate of the hot halo; the purple line is the outflow rate. The black dashed line denotes the halo mass accretion rate multiplied by the universal baryon fraction, $f_{b,0} = 0.17$. For comparison, the star formation rates inferred by Behroozi, Wechsler & Conroy (2013) and Lu et al. (2014a) using empirical models are over-plotted as the green and orange bands, respectively.

all the models are tuned to match the present-day stellar mass and cold gas mass of Milky-Way sized halos, it is not surprising that all models reproduce well the observed stellar and cold gas masses for $10^{12} M_{\odot}$ halos at $z = 0$. The measurements of hot halo gas mass have large uncertainties. Both Model-EJ and Model-PR can accommodate the observational results comfortably, while the prediction of Model-RI seems to be too high.

For $M_{\text{halo},0} = 10^{11} M_{\odot}$, both Model-EJ and Model-PR can achieve an excellent agreement with data for the final stellar mass, but Model-RI under-predicts the final stellar mass by a factor of 2 to 3. Even assuming strong outflows, both Model-EJ and Model-RI over-predict the cold gas mass by a factor of few. This over-prediction stems from the fact that a large amount of cold gas is settled in an extended gaseous disk where star formation is low due to the low surface density and feedback is not efficient to get rid of the cold gas. If we allow the gas disks to be smaller so that

star formation can occur in a larger fraction of the disk, the predicted gas mass can be reduced. However, as shown in Lu, Mo & Wechsler (2015), to match the cold gas mass requires disk sizes to be much smaller than real disks. We also note that the overproduction of cold gas mass causes an underprediction of gas-phase metallicity (see next section for details). When the gas-phase metallicity is sufficiently low, the star formation rate surface density strongly depends on the gas surface density. This nonlinear dependence causes an upturn in stellar mass in the final 2 Gyrs for $10^{11} M_{\odot}$ halo. In contrast to the ejective models, Model-PR can reproduce the stellar mass and cold gas mass for both $10^{12} M_{\odot}$ and $10^{11} M_{\odot}$ halos. In this model, the amount of cold gas settled in the outer parts of disks is smaller, as a large fraction of the gas is not able to make it to the disk because of preheating.

Figure 2 shows the rates at which the baryonic masses in different components transfer between each other. We focus on the cooling rate of halo gas, star formation rate

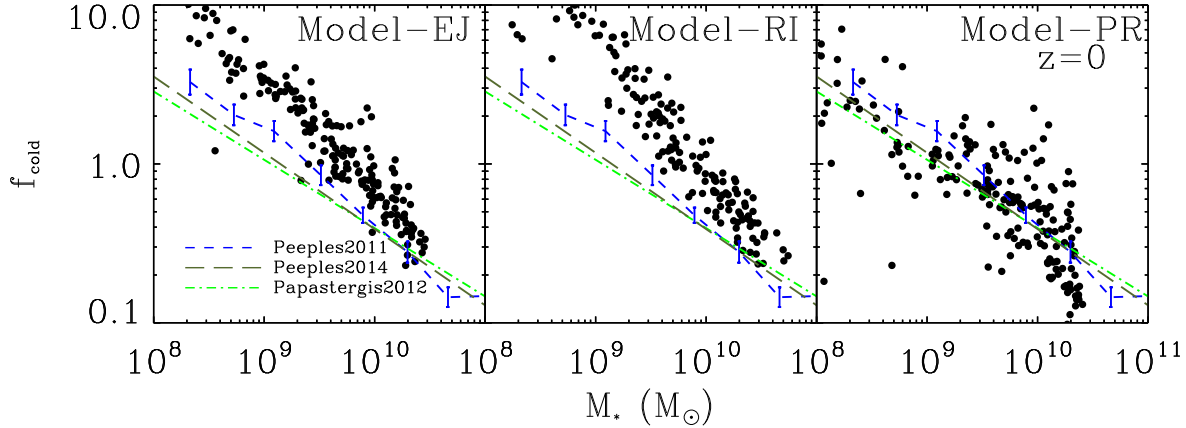


Figure 3. Cold gas mass - stellar mass ratio as a function of galaxy stellar mass at $z = 0$ predicted by different models, as labeled by their names in different panels. The mean relations derived from observational data by Peeples & Shankar (2011), Peeples et al. (2014), and Papastergis et al. (2012) are shown by different lines as noted in the figure.

of the cold gas, and the outflow rate as functions of time. For the outflow rate, we plot the rate at which the gas is leaving the galaxy. For Model-EJ, the outflow gas goes out of the halo, but for Model-RI a fraction of the outflow is retained in the halo. For simplicity, we do not distinguish between outflows going into the IGM and those going into the CGM. Since mass ejection is powered by star formation feedback in all the three models, the outflow rate is proportional to the SFR. The difference between models is in the assumed mass-loading factor. In Model-EJ, the mass-loading factor is proportional to V_{vir}^{-2} , and so low-mass halos have much higher outflow rate per star formation rate. Model-RI adopts a very large mass-loading factor to balance the gas re-incorporated into the gaseous halo, and so both the cooling rate and ejection rate are at least one order of magnitude higher than the SFR. In Model-PR, the cooling rate deviates significantly from the halo accretion rate because of preheating, and the star formation is largely controlled by the reduced rate of gas accretion. For comparison, we include the SFR as a function of time for both $M_{\text{halo},0} = 10^{11} M_{\odot}$ and $10^{12} M_{\odot}$, as inferred by Behroozi, Wechsler & Conroy (2013) and Lu et al. (2014a) from observational data. All the three models reproduce the average star formation history of $10^{12} M_{\odot}$ halos quite well. For $M_{\text{halo},0} = 10^{11} M_{\odot}$, Model-PR matches the empirical results well; Model-RI moderately under-predicts the SFR at low redshift; Model-EJ fails completely: it predicts too high a SFR at high z and too low a SFR at low z .

Figure 3 shows the present-day cold gas to stellar mass ratio f_{cold} as a function of galaxy stellar mass predicted by the three models. The predictions are made by applying the models to a random set of halo mass accretion histories selected from the Bolshoi cosmological N -body simulation (Klypin, Trujillo-Gomez & Primack 2011) for the mass range between 10^{10} and $10^{12} M_{\odot}$. As one can see, the gas fractions predicted by all the three models for high mass halos are consistent with observational results. This again is because the model parameters are all tuned to match the properties of Milky Way sized galaxies. Both of the ejective

models (Model-EJ and Model-RI) predict a steep decline of the gas fraction with stellar mass, so that both models significantly over-predict the gas fractions in low-mass galaxies. Varying the normalization of the mass-loading factor in the ejective models only shifts the amplitude of the predicted relation but has negligible effect on the slope of the relation, and so cannot fix the mismatch. In contrast, Model-PR reproduces the observed $f_{\text{cold}}-M_*$ relation quite well. This model predicts a large scatter in the cold gas fraction for high-mass galaxies. This is largely caused by the ‘late quenching’ we introduced, in which the suppression of gas cooling depends strongly on stellar mass. Also, star formation in halos less massive than $10^{11} M_{\odot}$ depends sensitively on halo mass accretion history in this model. Depending on whether a halo has acquired most of its mass before or after the onset of preheating, the total amount of stars that can form can be very different. This has the effect of increasing the scatter in the predicted $f_{\text{cold}}-M_*$ relation.

4 METAL MASSES AND METALLICITIES IN DIFFERENT GAS COMPONENTS

We also follow the histories of the metal mass in stars, cold gas, hot halo gas, and ejected gas of model galaxies hosted by $10^{11} M_{\odot}$ and $10^{12} M_{\odot}$ halos. we adopt the usual instantaneous recycling approximation for metals produced by star formation to be returned to ISM and CGM. The time delays between the nuclear synthesis of different heavy elements are ignored for simplicity. This approximation is supported by the results of Peeples et al. (2014), who showed that the Oxygen mass, which is mainly produced by Type II SNe, is roughly a constant fraction of the total metal mass over the stellar mass range of our study. Figure 4 shows the histories of metal mass in each component as a function of time (redshift) predicted by the three models. In each panel, we also show the total available metal mass, $pM_*/(1-R)$ (with p being the metal yield and R the return fraction), as star formation proceeds. We adopt $R = 0.43$, which is proper for a

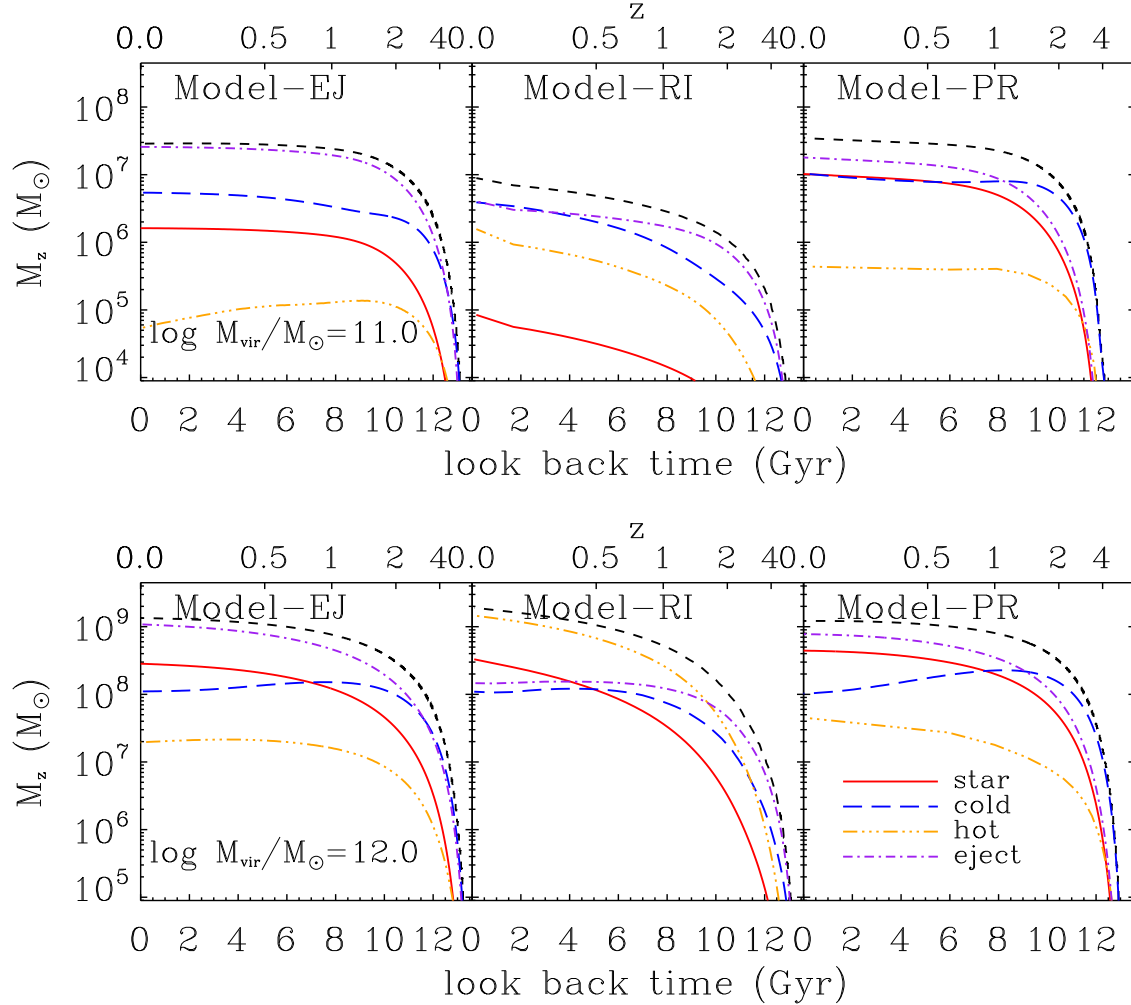


Figure 4. The metal masses in different phases of baryonic matter as predicted by the three models (EJ, RI and PR, as indicated in the panels) for halos with final masses of $10^{12} M_{\odot}$ (lower panels) and $10^{11} M_{\odot}$ (upper panels) at the present day. The red lines are for the metal masses locked in stars, the blue lines for metals in cold gas, the orange lines for metals in gaseous halo, and the purple lines for metals that are ejected out of halo. The black dashed lines denote the metal mass available for the galaxy, which is approximated by $p \frac{M_{*}}{1-R}$.

Chabreir IMF. The ejective feedback in Model-EJ expels the enriched gas from the galaxy, and so most of the metal mass ends up in the ejected gas. In Model-RI, the ejected mass returns back to the halo after a short time delay for the Milky Way sized halo, but can stay in the halo for a longer period of time. Consequently, most of the metal mass in such a halo is in the hot halo gas. For $10^{11} M_{\odot}$ halos, on the other hand, the ejected component contains a larger fraction of metals than the halo gas, because gas re-incorporation is slow for low-mass halos and much of the ejected gas stays outside of the halo. Furthermore, since low-mass halos are predicted to have a high cold gas fraction, the cold gas in such a halo is predicted to contain a large fraction of the total metal mass in Model-RI. In contrast, Model-PR predicts that the metal masses locked in stars and cold gas are always a substantial fraction of the total, while the metal mass in the halo gas is lower by a factor of a few.

In Figure 5 we show the metal masses in different phases versus stellar mass for galaxies at $z = 0$ predicted by the

three models, and compare the model predictions with the compilation of observational data by Peebles et al. (2014). In addition, we also include a horizontal bar to represent the observational estimate of metal mass in hot halos derived from OVI absorptions of COS-Halos samples, assuming $p_{oxy} = 0.44p$ and the same ionization fraction $f_{\text{OVI}} = 0.2$ as adopted in Tumlinson et al. (2011). All the models predict that the metal mass increases with stellar mass, except for the ejected mass predicted by Model-RI. The general increasing trend is set by the total metal mass available, which is plotted as the black dashed line in the figure. Galaxies with higher stellar masses can produce more metals, but where the metals are located depends strongly on the feedback model.

In Model-EJ, a substantial fraction of the ISM is blown out of galaxies, and because all the ejected mass is assumed to leave the halo forever, most of the metal mass is predicted in the ejected component for galaxies of different masses. The model also has a small fraction of metals in the hot gas,

which stems from our assumption that a fraction of metal yield is deposited in the halo. For the particular parameter ($\alpha_Z = 0.1$) assumed here, the predicted metal mass in the hot halo is about $2 \times 10^7 M_\odot$ for galaxies with final stellar masses $\sim 10^{10} M_\odot$, which is consistent with the observational results (Tumlinson et al. 2011). The predicted metal mass in the cold gas component also matches well the observational data presented in Peeples et al. (2014). We note that increasing α_Z can increase the metal mass in the hot gas to make the model prediction agree with the data better, but it will lower the metal mass in the cold gas component so that the agreement with the observational results does not hold anymore. Overall, this model nicely reproduces the metal masses as functions of galaxy stellar mass in all components, except the ejected component, for which data constraint is not available.

Model-RI predicts a trend of the metal mass in stars and cold gas that is similar to that in Model-EJ due to the common assumption of ejective feedback. However, the two models predict very different trends for the metal mass in the hot gas and the ejected gas. Since the reincorporation is fast for high-mass galaxies (Henriques et al. 2013), a large fraction of metals can return back to the hot halo. Consequently, the predicted metal mass in the ejected component first increases with increasing stellar mass, and then decreases, for galaxies with stellar masses $> 10^{10} M_\odot$. The metal mass in the halo gas predicted by this model increases rapidly with increasing galaxy mass owing to both the increase of total metal production and the halo mass-dependent reincorporation. Furthermore, since a large fraction of metals stays in the halo, the model predicts high metal mass in the cold phase, especially for low-mass halos where cooling from the halo gas is efficient.

Model-PR adopts a moderate ejection with a mass-loading factor equal to unity, and Fig. 5 shows that even with such a small loading factor the ejected mass can still contain a large fraction of all the produced metals. Most of the metals that are not ejected are predicted to be locked in stars and cold disk gas. As in Model-RI, metals in the hot halo gas are due to the assumed direct deposition in the halo. Again, we see that for the particular choice of $\alpha_Z = 0.1$, the model predicts about $10^7 M_\odot$ of metals in the halo of a galaxy with $M_* = 10^{10} M_\odot$, which is consistent with the observational results. The predicted metal mass in cold gas matches the observation result, but the model seems to over-predict the metal mass in stars. As we will discuss in the following section, this discrepancy is the only main problem for this model, and suggests that the assumption of uniform mixing of metals in the ISM may be invalid.

The relation between the gas-phase metallicity and galaxy stellar mass has been studied observationally over the redshift range $0 < z < 3$ by many authors (Tremonti et al. 2004; Erb et al. 2006; Maiolino et al. 2008, e.g.). However, hydrodynamic simulations and semi-analytic models of galaxy formation have difficulty in reproducing the relation over the redshift range probed by the observation (De Lucia, Kauffmann & White 2004; de Rossi, Tissera & Scannapieco 2007; Mouhcine et al. 2008). In Figure 6 we show the predictions of our three models for the oxygen metallicity in cold disk gas at three different redshifts, $z = 0, 1$, and 2. For comparison, we plot three sets of observational results obtained

by Andrews & Martini (2013), Maiolino et al. (2008), Zahid et al. (2013), Yabe et al. (2012) and Erb et al. (2006). The ejective feedback model (Model-EJ) predicts only a weak evolution in the oxygen metallicity - stellar mass relation from $z = 2$ to the present day, which is at odd with the increase of the metallicity with time for a fixed stellar mass shown in the observational data (Mannucci et al. 2009; Maiolino et al. 2008; Mannucci et al. 2010; Zahid et al. 2013). The predicted metallicities at low redshifts are too low to match the observation. The reason for this is twofold. First, the model over-predicts the cold gas fraction for a given stellar mass, which leads to a reduced metallicity for the gas. Second, metals are also ejected out of galaxies with outflow, further reducing the metallicity. The under-prediction and the lack of evolution also appear in Model-IR. Henriques et al. (2013) found that their reincorporation model can match the *stellar* metallicity - stellar mass relation for local galaxies, assuming a metal yield $p = 0.047$ that is 60% higher than what is assumed here. However, our results show that the reincorporation model is not able to reproduce the evolution in the gas phase metallicity unless p is time-dependent. The preheating model Model-PR predicts a moderate level of evolution and a large scatter in the gas phase metallicity for given stellar mass, and the model predictions are consistent with the observational data assuming $p = 0.03$.

Since we assume that metals in the halo gas is perfectly mixed in a density profile, we can make predictions for the column density of any chemical species as a function of the impact parameter (distance from galaxy center). The COS-Halos survey has measured the OVI column density profile for a sample of L^* galaxies around redshift $z = 0.4$. Here we make the corresponding predictions for a $10^{12} M_\odot$ halo at $z = 0.4$ and compare our model predictions with the data. In the calculation, we follow Tumlinson et al. (2011) and assume that the ionization fraction of OVI, $f_{\text{OVI}} = 0.2$. As shown in Fig. 7, all the three models can roughly reproduce the shape of the column density profile. The predictions of Model-EJ and Model-PR agree with the data reasonably well, but the column density profile predicted by Model-RI is about 2 orders of magnitude too high. This over-prediction by Model-RI is again due to the reincorporation of the ejected gas, which is enriched in metal.

Werk et al. (2014) have estimated the mass and column density profile of cool gas in the circum-galactic medium for 44 Milky Way sized galaxies in the COS-Halos sample. They found that the total amount of cool gas (with temperature in the range $10^4 \text{ K} < T < 10^5 \text{ K}$) is larger than about $6.5 \times 10^{10} M_\odot$, and that the cool gas column density profile can be well described by a shallow power-law with a power index ~ -1 or lower. Assuming the cooling halo gas in our model to be this cool component in the circum-galactic medium, we compare our model predictions for a typical $10^{12} M_\odot$ halo at $z = 0.2$ with the observational results. To do this, we estimate the amount of the halo gas at different radii that can cool in a given time interval based on the profile of the hot halo gas. The gas cools from a shell at radius r_i covers a $4\pi r_i^2$ area. Assuming that the cooled gas falls onto the halo center in one free-fall time from the radius with a constant speed, the cool halo gas that drops from radius r_i has a radial distribution proportional to $\frac{1}{r^2}$, where $r < r_i$. Thus, the total mass density of the cooled halo gas from all

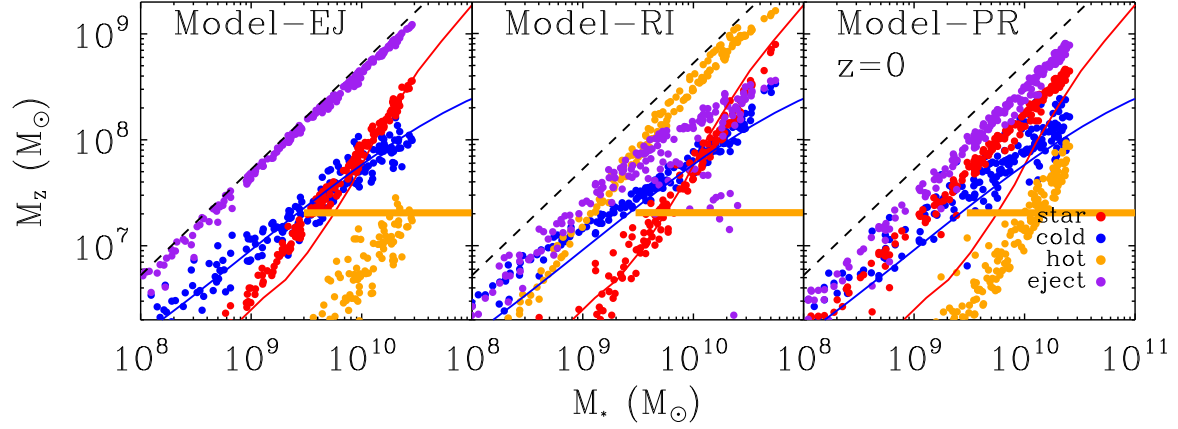


Figure 5. The relation between metal mass in different baryonic mass components and the stellar mass for model galaxies predicted by different models. The model name is noted in each panel. The red dots denote metal mass locked in stars, the blue dots denote metal mass in cold gas in galaxies, and orange dots denote metal mass in hot halo, and the purple dots denote metal mass in gas that is ejected out of the halos. The horizontal orange bar marks the observational estimate of the metal mass in halo gas around galaxies with masses over the range of stellar masses covered by the bar as measured in COS-Halos through OVI line (Tumlinson et al. 2011). Solar oxygen abundance pattern is assumed.

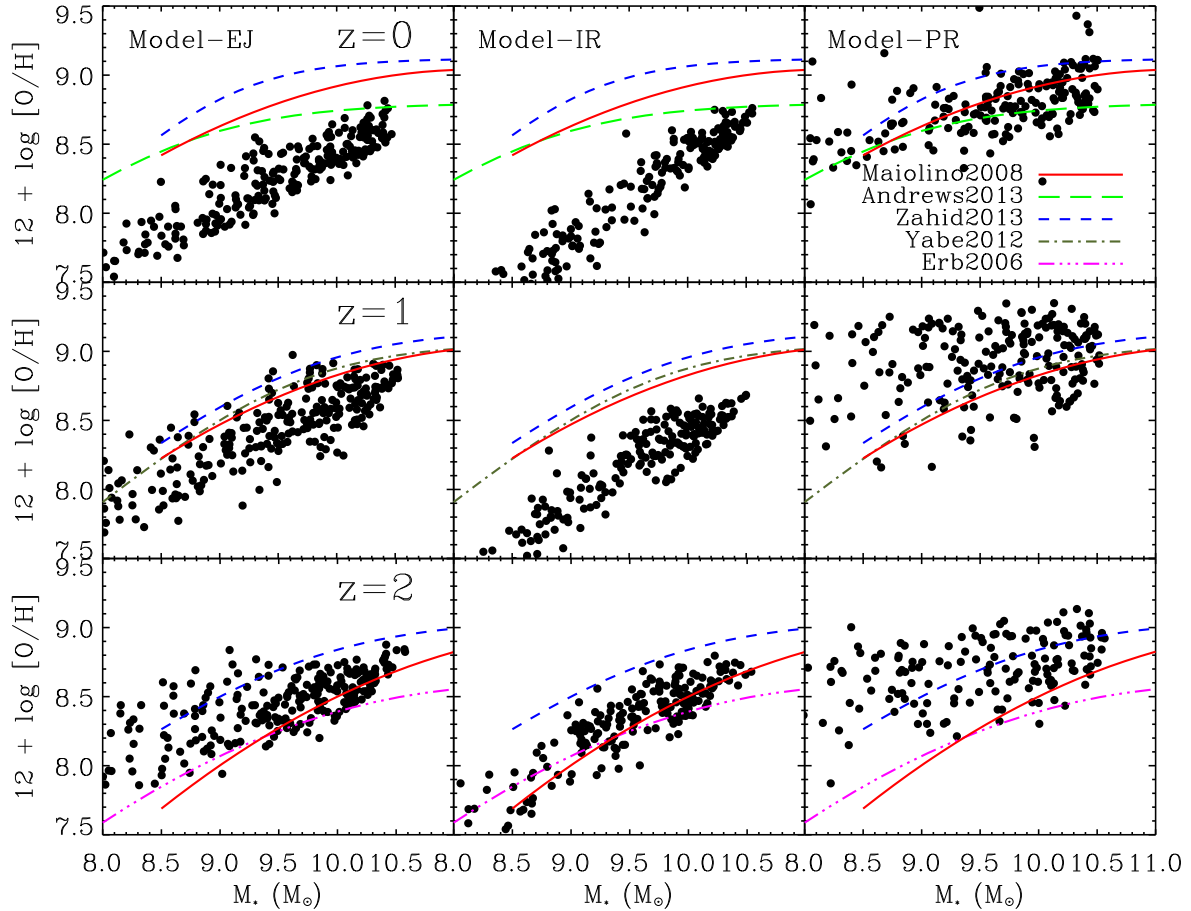


Figure 6. The metallicity of the cold gas (ISM) as a function of stellar mass at $z = 0, 0.5, 1,$ and 2 predicted by Model-EJ, Model-IR, and Model-PR. The fitting functions of the mean relations derived from the observational data of Andrews & Martini (2013); Maiolino et al. (2008), Zahid et al. (2013), Yabe et al. (2012) and Erb et al. (2006) are shown in each corresponding panel for comparison.

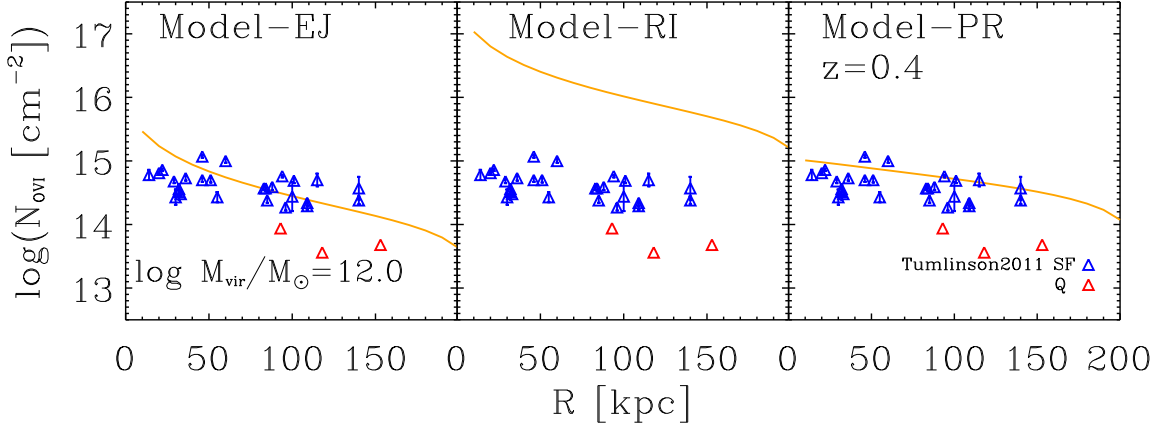


Figure 7. The column density of OVI as a function of impact parameter (projected radius from galaxy center) for a $10^{12} M_{\odot}$ halo predicted by different models. The blue data points are observational data for star forming galaxies and the red data points are for quiescent galaxies obtained in Tumlinson et al. (2011).

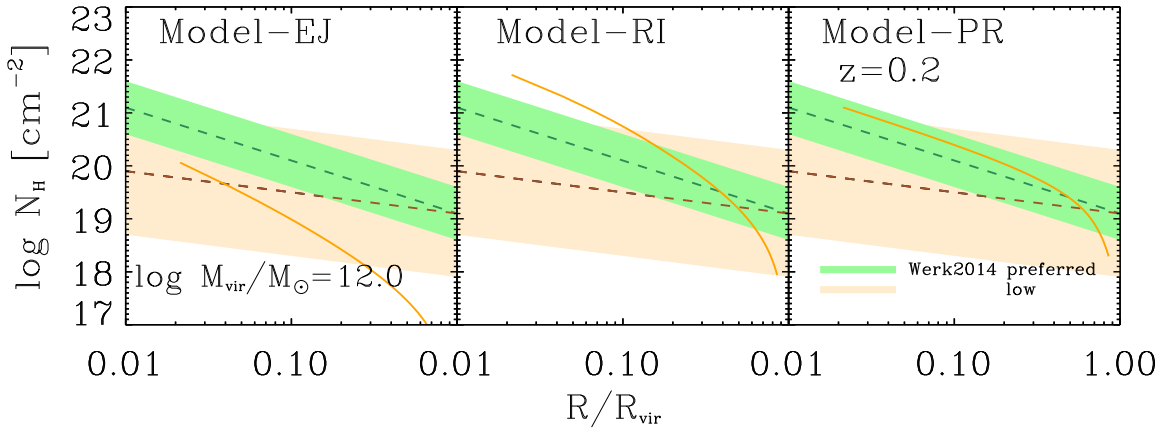


Figure 8. The cooling gas column density as a function of impact parameter (projected radius from galaxy center) for a $10^{12} M_{\odot}$ halo predicted by different models. The green and orange bands represent the ‘preferred’ and lower limits of the observational estimates of Werk et al. (2014).

the outer shells at a radius r can be written as

$$\rho_{\text{cool}}(r) = \frac{1}{r^2} \int_r^{R_{\text{vir}}} \Lambda(r_i) \tau_{\text{ff}}(r_i) r_i dr_i, \quad (8)$$

where $\Lambda(r_i)$ is the cooling rate of the halo gas per unit volume at r_i , and τ_{ff} is the free-fall time of the gas element from the radius where it cools. The free-fall time is estimated as

$$\tau_{\text{ff}} = 14.4 \text{Gyr} \left(\frac{r_i}{1 \text{Mpc}} \right)^{\frac{3}{2}} \left[\frac{M(< r_i)}{10^{12} M_{\odot}} \right]^{-\frac{1}{2}}, \quad (9)$$

where $M(< r_i)$ is the total mass (dark matter and baryon) within radius r_i . We then calculate the column density from the radial profile and the cool gas column density profiles predicted by the three different models, which are shown in Fig. 8. The amplitudes of the column density profiles predicted by both Model-EJ and Model-PR agree with the observational results, while that predicted by Model-IR seems

too high. These are consistent with the predicted cooling rates shown in Fig. 2: Model-EJ and Model-PR predict a much lower rate than Model-IR. More interestingly, both ejective feedback models predict profiles that are significantly steeper than the observational estimates. In contrast, the preheating model predicts an extended cooling gas profile similar to the observational results.

5 DISCUSSION AND SUMMARY

Using a set of semi-analytic models of galaxy formation, we have demonstrated that the gas and metal contents of the galaxy population provide important constraints on the feedback processes assumed in galaxy formation models. In particular, the masses and the metallicities of baryonic

Mass Scale	Quantity	Model-EJ	Model-RI	Model-PR	Figure
$M_{\text{vir}} = 10^{11} M_{\odot}$	$M_*(z=0)$	OK	too low	OK	1
	$M_{\text{cold}}(z=0)$	too high	too high	OK	1
	SFH	too low at low-z	too low at low-z	OK	2
	$f_{\text{cold}}(z=0)$	too high	too high	OK	3
$M_{\text{vir}} = 10^{12} M_{\odot}$	$M_*(z=0)$	OK	OK	OK	1
	$M_{\text{cold}}(z=0)$	OK	OK	OK	1
	SFH	OK	OK	OK	2
	$f_{\text{cold}}(z=0)$	OK	OK	OK	3
$M_* = 10^8 - 10^{10.5} M_{\odot}$	$Z_{\text{ISM}}(z=0)$	too low	too low	OK	6
	$Z_{\text{ISM}}(z=2)$	OK	OK	OK	6
	$M_{Z,*}(z=0)$	OK	OK	too high	5
	$M_{Z,\text{hot}}$	OK	too high	OK	5,7

Table 1. A summary of the success and failure of the three models based on comparisons with different observational data. The first column lists the masses of model halos or galaxies. The second column lists the quantities in the comparison. The third to fifth columns list the performances of the three models. The last column lists the corresponding figures from which the conclusion is drawn.

matter in different phases can be used to distinguish two broad classes of feedback scenario, namely ejective and preventative feedback. We have found that when the models are tuned to predict a correct stellar mass for a given halo mass, different feedback mechanisms work differently in redistributing the metal-enriched material, and hence predict very different trends for metallicities.

We have considered three representative models. Two of them implement ejective feedback, in which halos accrete baryonic matter together with dark matter at the cosmic baryon fraction. To match the observed stellar mass fraction of galaxies in the ejective scenario, a significant fraction of baryonic matter that cools into the central galaxy has to be ejected out of the galaxy by star formation feedback. One of the ejective models implements a simple assumption that the ejected material never comes back, while the other one considers a more sophisticated model in which the ejected gas can be re-incorporated into the halo. The third model implements a preventative feedback model, in which feedback works to preheat the IGM, and the thermal pressure prevents a fraction of baryon from collapsing into low-mass halos. To explore the characteristics of these models, we have contrasted their predictions in the masses and metallicities of stars, cold disk gas, hot halo gas, and ejected gas. Table 1 summarizes the success and failure of the model predictions in comparison with existing observational data. In the following we discuss the implications of these results.

First, ejective and preventative models predict different fractions of baryons that reside in a halo and outside the halo virial radius. The pure ejective model predicts that most of the baryon mass is ejected out of the halo, and only a small fraction is retained in the central galaxy and the halo. The ejective model with gas reincorporation has similar predictions for low-mass halos, but for Milky Way sized galaxies it predicts that the dominating fraction of baryons is in the halo because the ejected gas can return quickly back to the halo.

Second, we have shown that when the outflow mass-loading parameter is tuned to be large enough in the ejective models so that the predicted total stellar mass matches the

observed stellar mass - halo mass relation, model galaxies tend to have too high a gas mass fraction compared with observational data. Meanwhile, the ejective models also predict a too low gas-phase metallicity. Although stronger outflow with an even larger mass-loading factor could reduce the gas fraction in the ejective models, the metal mass will inevitably decrease further, resulting in an even lower gas-phase metallicity. Thus, the ejective models appear to be unable to accommodate the observed gas/stellar mass fraction and gas-phase metallicity simultaneously.

Third, regardless of the details of how ejection and reincorporation are parameterized, the ejective models always predict a gas phase metallicity-stellar mass relation with roughly fixed amplitude and slope since $z = 2$ without strong time evolution, which is inconsistent with current observations.

Finally, we have shown that if feedback is primarily ejective and the ejected mass can be reincorporated into massive halos rapidly as suggested in recent models (e.g. Henriques et al. 2013), gaseous halos may contain too much metal mass to be consistent with COS-Halos observational results.

In contrast the preventative model can accommodate almost all observational data, including the evolution of masses and metallicities of baryonic matter in different phases. The only problem is that the model predicts too high metal masses in the stellar component of low-mass galaxies. Given that this model predicts the correct metal mass in ISM, and the correct total stellar and cold gas masses, the problem cannot be solved by assuming stronger outflows with uniform mixing. The over-prediction suggests that a significant fraction of stars in low-mass galaxies may form in a medium with a significant lower metallicity than the average ISM metallicity. This can happen if a fraction of star formation in low-mass galaxies occurs in early starburst before $z = 2$, when the ISM metallicity has not been substantially enriched (Lu et al. 2014b). Alternatively, a large fraction ($> 70\%$) of the stellar mass in low-mass galaxies may have formed in regions where the metallicity is lower than the average. Indeed, as demonstrated in detail in Lu et

al. (2015, submitted), both the observed stellar-phase metallicity and gas-phase metallicity as functions of galaxy stellar mass can be reproduced, if star formation occurs in an ISM with inhomogeneous metallicity, where a large fraction of the star forming ISM has metallicities below the average ISM metallicity. Since real ISM is inhomogeneous in metallicity (Smartt & Rolleston 1997; Ho et al. 2015), this only discrepancy for the preventative model may not be a real problem after all.

In summary, the results we have obtained indicate that the basic assumption of the ejective model that all baryonic matter first collapses into a halo and the baryonic matter budget in a galaxy is regulated by outflows is problematic. This, together with the success of the preventive model considered here and in Lu, Mo & Wechsler (2015), suggests that feedback is likely preventative in nature. In the present paper we have explored the different models by manually varying the key model parameters. These parameters certainly have degeneracy between them. In addition, the two processes, ejection and prevention, are expected to be degenerate to some extent for some of the observational constraints. It remains to be revealed how these two processes are degenerate and what observational data can effectively break the degeneracy. We will investigate these questions using the Bayesian model inference approach developed by Lu et al. (2011) in a future paper.

ACKNOWLEDGEMENT

The authors thank Andrew Benson, Guillermo Blanc, Mike Fall, Yicheng Guo, Rachel Somerville, Risa Wechsler for useful discussions. YL received partial support from HST-AR-12838, provided by NASA through a grant from the Space Telescope Science Institute, which is operated by the Association of Universities for Research in Astronomy, Inc., under NASA contract NAS5-26555. HJM acknowledges the support from NSF AST-1109354. This work used the Extreme Science and Engineering Discovery Environment (XSEDE), which is supported by National Science Foundation grant number ACI-1053575.

REFERENCES

- Allende Prieto C., Lambert D. L., Asplund M., 2001, *ApJL*, 556, L63
- Andrews B. H., Martini P., 2013, *ApJ*, 765, 140
- Asplund M., Grevesse N., Sauval A. J., Scott P., 2009, *ARA&A*, 47, 481
- Behroozi P. S., Conroy C., Wechsler R. H., 2010, *ApJ*, 717, 379
- Behroozi P. S., Wechsler R. H., Conroy C., 2013, *ApJ*, 770, 57
- Benson A. J., Frenk C. S., Baugh C. M., Cole S., Lacey C. G., 2003, *MNRAS*, 343, 679
- Benson A. J., Madau P., 2003, *MNRAS*, 344, 835
- Bouché N., Hohensee W., Vargas R., Kacprzak G. G., Martin C. L., Cooke J., Churchill C. W., 2012, *MNRAS*, 426, 801
- Bower R. G., Benson A. J., Malbon R., Helly J. C., Frenk C. S., Baugh C. M., Cole S., Lacey C. G., 2006, *MNRAS*, 370, 645
- Bregman J. N., Lloyd Davies E. J., 2007, *ApJ*, 669, 990
- Croton D. J. et al., 2006, *MNRAS*, 367, 864
- De Lucia G., Kauffmann G., White S. D. M., 2004, *MNRAS*, 349, 1101
- de Rossi M. E., Tissera P. B., Scannapieco C., 2007, *MNRAS*, 374, 323
- Dekel A. et al., 2009, *Nature*, 457, 451
- Dekel A., Silk J., 1986, *ApJ*, 303, 39
- Erb D. K., Shapley A. E., Pettini M., Steidel C. C., Reddy N. A., Adelberger K. L., 2006, *ApJ*, 644, 813
- Fang T., Mckee C. F., Canizares C. R., Wolfire M., 2006, *ApJ*, 644, 174
- Guo Q. et al., 2011, *MNRAS*, 413, 101
- Gupta A., Mathur S., Krongold Y., Nicastro F., Galeazzi M., 2012, *ApJL*, 756, L8
- Henriques B. M. B., White S. D. M., Thomas P. A., Angulo R. E., Guo Q., Lemson G., Springel V., 2013, *MNRAS*, 431, 3373
- Ho I., Kudritzki R.-P., Kewley L. J., Zahid H. J., Dopita M. A., Bresolin F., Rupke D. S. N., 2015, *ArXiv e-prints*
- Kacprzak G. G. et al., 2014, *ApJL*, 792, L12
- Kang X., Jing Y. P., Silk J., 2006, *ApJ*, 648, 820
- Klypin A. A., Trujillo-Gomez S., Primack J., 2011, *ApJ*, 740, 102
- Lu Y., Mo H. J., 2007, *MNRAS*, 377, 617
- Lu Y., Mo H. J., Wechsler R. H., 2015, *MNRAS*, 446, 1907
- Lu Y., Mo H. J., Weinberg M. D., Katz N., 2011, *MNRAS*, 416, 1949
- Lu Z., Mo H. J., 2014, *ArXiv e-prints*: 1407.4382
- Lu Z., Mo H. J., Lu Y., 2014, *ArXiv e-prints*: 1408.2640
- Lu Z., Mo H. J., Lu Y., Katz N., Weinberg M. D., van den Bosch F. C., Yang X., 2014a, *MNRAS*, 439, 1294
- Lu Z., Mo H. J., Lu Y., Katz N., Weinberg M. D., van den Bosch F. C., Yang X., 2014b, *ArXiv e-prints*: 1406.5068
- Maiolino R. et al., 2008, *A&A*, 488, 463
- Mannucci F., Cresci G., Maiolino R., Marconi A., Gnerucci A., 2010, *MNRAS*, 408, 2115
- Mannucci F. et al., 2009, *ApJ*, 398, 1915
- McBride J., Fakhouri O., Ma C.-P., 2009, *MNRAS*, 398, 1858
- Mo H. J., Mao S., 2002, *MNRAS*, 333, 768
- Mo H. J., Mao S., 2004, *MNRAS*, 353, 829
- Mo H. J., Yang X., van den Bosch F. C., Katz N., 2005, *MNRAS*, 363, 1155
- Moster B. P., Naab T., White S. D. M., 2013, *MNRAS*, 428, 3121
- Mouhcine M., Gibson B. K., Renda A., Kawata D., 2008, *A&A*, 486, 711
- Oh S. P., Benson A. J., 2003, *MNRAS*, 342, 664
- Papastergis E., Cattaneo A., Huang S., Giovanelli R., Haynes M. P., 2012, *ApJ*, 759, 138
- Peeples M. S., Shankar F., 2011, *MNRAS*, 417, 2962
- Peeples M. S., Werk J. K., Tumlinson J., Oppenheimer B. D., Prochaska J. X., Katz N., Weinberg D. H., 2014, *ApJ*, 786, 54
- Smartt S. J., Rolleston W. R. J., 1997, *ApJL*, 481, L47
- Somerville R. S. et al., 2008, *ApJ*, 672, 776
- Tremonti C. A. et al., 2004, *ApJ*, 613, 898
- Tumlinson J. et al., 2011, *Science*, 334, 948
- van den Bosch F. C., 2002, *MNRAS*, 331, 98

- van den Bosch F. C., Abel T., Hernquist L., 2003, *MNRAS*, 346, 177
- Wechsler R. H., Bullock J. S., Primack J. R., Kravtsov A. V., Dekel A., 2002, *ApJ*, 568, 52
- Werk J. K. et al., 2014, *ApJ*, 792, 8
- Yabe K. et al., 2012, *Publications of the Astronomical Society of Japan*, 64, 60
- Yang X., Mo H. J., van den Bosch F. C., 2003, *MNRAS*, 339, 1057
- Yao Y., Nowak M. A., Wang Q. D., Schulz N. S., Canizares C. R., 2008, *ApJL*, 672, L21
- Zahid H. J., Geller M. J., Kewley L. J., Hwang H. S., Fabricant D. G., Kurtz M. J., 2013, *ApJ*, 771, L19
- Zhao D. H., Jing Y. P., Mo H. J., Börner G., 2003a, *ApJL*, 597, L9
- Zhao D. H., Jing Y. P., Mo H. J., Börner G., 2009, *ApJ*, 707, 354
- Zhao D. H., Mo H. J., Jing Y. P., Börner G., 2003b, *MNRAS*, 339, 12